

MECHANISMS OF SCREECH MODE STAGING IN UNDEREXPANDED SUPERSONIC JETS

Soudeh Mazharmanesh[1], Joel Weightman[1], Petr^onio A. S. Nogueira[1] & Daniel Edgington-Mitchell[1]

[1]Monash University, Department of Mechanical and Aerospace Engineering

Abstract

This study investigates the screech staging mechanism associated with different axisymmetric modes in off-design supersonic jets. While staging phenomena have previously been examined using time–frequency analysis techniques, most studies have primarily focused on characterising the multimodal behaviour during staging, specifically whether modes coexist or switch in a mutually exclusive manner. However, the underlying physical mechanism responsible for transitions between screech modes remains insufficiently understood. In the present work, we investigate the physical mechanism responsible for switching between the A1 and A2 screech modes in an underexpanded axisymmetric jet experimentally. High-speed schlieren visualisations are analysed using Hilbert proper orthogonal decomposition (HPOD) to characterise the temporal dynamics of the screech modes. The results show that, although the dominant behaviour consists of alternating switching between A1 and A2 modes, there exist finite intervals during which both modes coexist simultaneously at low amplitude. Our findings demonstrate that, when the A1 and A2 modes are mutually exclusive, the activation of each mode modifies the mean flow through triadic self-interaction. This mean-flow modification is characterised by changes in the shock-cell spacing relative to the long-time mean flow. We show that, when one screech mode becomes dominant, the resulting variation in shock-cell spacing alters the mean flow in a manner that satisfies the resonance closure condition for the alternate mode, thereby triggering its emergence. These findings provide new insight into the amplitude dynamics, nonlinear energy transfer, and mean-flow modification mechanisms underlying A1–A2 screech staging, with important implications for understanding mode transitions and developing strategies for noise control in underexpanded supersonic jets.

Keywords: Aeroacoustics, Jet noise, Shock waves, Screech, Mode staging

1. Introduction

Supersonic jets operating under off-design conditions generate an additional shock-associated noise source beyond turbulent mixing noise. This shock-associated noise may appear as broadband radiation or as a discrete tonal component known as screech [1], which can adversely affect aircraft structures [2] and pose hearing hazards to personnel working near high-speed jets [3]. The screech mechanism was first described by [4] as a resonance loop involving downstream-propagating instability waves, the shock-cell structure, and upstream-propagating disturbances. Subsequent developments led to the weakest-link model, in which screech arises from the interaction between the Kelvin–Helmholtz (KH) wavepacket and the quasi-periodic shock-cell structure [5, 6]. More recently, the model has been refined by recognising the role of guided jet modes as the upstream-propagating disturbance [7]and by accounting for spatial variations in shock-cell spacing that govern the resonance closure mechanism [8]:

$$k_{GJM} = k_{kh} - k_{s_{1,2,3}}, \tag{1}$$

where k_{s_1} denotes the primary wavenumber peak and $k_{s_{2,3}}$ represent the suboptimal peaks of the shock-cell structure.

One of the characteristic features of screech is mode staging, where small changes in jet operating conditions produce abrupt transitions between discrete screech frequencies [9, 10, 11]. Near staging boundaries, multiple screech modes may exist at the same operating condition, either coexisting simultaneously or switching in a mutually exclusive manner. In axisymmetric jets, the A1–A2 transition is of particular interest because both modes remain axisymmetric and differ only in their resonance closure mechanism. Previous studies have shown that the A1 mode is associated with the primary shock-cell wavenumber, whereas the A2 mode is linked to a secondary shock-cell wavenumber generated by streamwise variations in shock spacing [8]. Although this explains the observed frequency shift, the physical mechanism responsible for switching between the two modes remains poorly understood.

Time–frequency analyses have provided valuable insight into the temporal behaviour of screech staging, demonstrating that A1 and A2 often switch in a mutually exclusive manner [12, 2, 13, 14, 15, 16]. However, these studies have largely focused on characterising multimodal behaviour rather than explaining why transitions between screech modes occur. Because the resonance closure condition depends on the mean flow, any mechanism capable of modifying the mean flow has the potential to alter the resonance process and trigger mode switching. Our recent work [17] has shown that nonlinear triadic self-interactions of screech modes generate distinct short-time mean-flow states associated with individual screech modes. These observations suggest that mean-flow distortion may provide the missing link between nonlinear modal interactions and screech staging, although its causal role in mode switching has yet to be established.

The objective of the present study is to investigate the physical mechanism governing A1–A2 screech staging in an underexpanded supersonic jet. High-speed schlieren visualisations are analysed using spectral proper orthogonal decomposition (SPOD) and Hilbert proper orthogonal decomposition (HPOD) to characterise the temporal behaviour of the screech modes, their triadic interactions, and associated mean-flow modifications. The paper is structured as follows: the experimental setup and analysis techniques are described in Sections 2. and 3., respectively. Results are presented in Sections 4. and 5., and conclusions are drawn in Section 6..

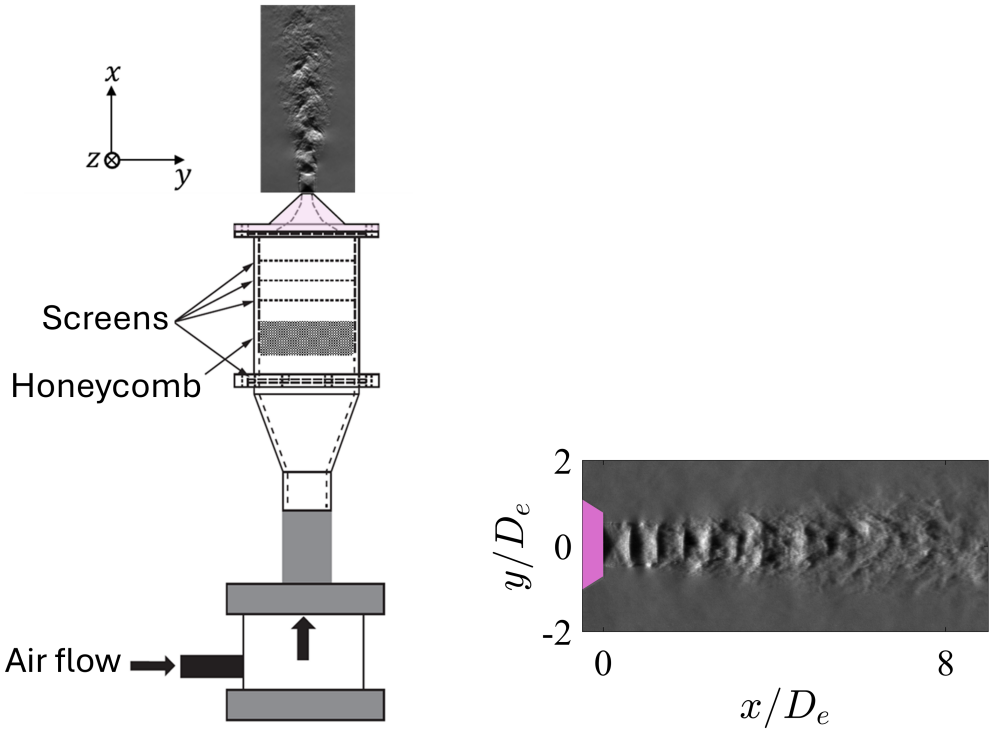
2. Experimental set-up

The experiments were performed in the Supersonic Gas-Jet Facility at the Shock Lab, Monash University. A schematic of the experimental configuration is shown in figure 1(a). The facility provides a continuous supply of high-pressure air and was operated at a nozzle pressure ratio of $\mathrm{NPR} = 2.2$, defined as the ratio of plenum pressure to ambient pressure. The flow is conditioned upstream of the nozzle using a combination of honeycomb structures and screens installed within the plenum chamber before being discharged through a purely convergent axisymmetric nozzle with an exit diameter of $D = 16.0$ mm and a non-dimensional lip thickness of $l/D = 0.31$.

Flow visualisation of the supersonic jet is performed using a Z-type Toepler schlieren arrangement, consisting of two mirrors with a focal length of 2032 mm to generate a collimated light beam across the test section. Image acquisition is carried out with a Photron Fastcam SA-Z 2100k at a frame rate of $150{,}000$ frames per second and a spatial resolution of 512×200 pixels. A pulsed light-emitting diode (LED) [18], with a pulse duration of $0.5, \mu s$, is used as the illumination source, enabling the recording of approximately $400{,}000$ frames per operating condition. The recorded intensity field is proportional to the path-integrated streamwise density gradient, $(\partial \rho_l / \partial x)$. Figure 1(b) illustrates the semi-axis aligned with the schlieren line of sight, along with representative instantaneous schlieren images of the axisymmetric jet at $\mathrm{NPR} = 2.20$.

3. Data decomposition

In this study, two modal decomposition techniques, SPOD and HPOD are employed to analyse the schlieren data. SPOD [19, 20, 21, 22] isolates the most energetic coherent structures at given fre-



(a) (b)

Figure 1 – (a) Schematic of the supersonic-jet experimental facility. (b) Instantaneous schlieren image of an axisymmetric jet operating at $\mathrm{NPR} = 2.20$.

quencies. It is used here to identify the screech modes ξ and the corresponding SPOD eigenvalues λ at the screech frequencies, based on light-intensity data extracted from schlieren images. Details of the mathematical formulation and implementation are provided in [21].

Hilbert proper orthogonal decomposition (HPOD) extends the classical POD framework by producing complex-valued modes that are suitable for modeling oscillatory behavior [23, 24, 25]. HPOD utilizes the analytic signal concept, transforming a flow-field time series into a complex representation via the Hilbert transform [26], which introduces an imaginary component phase-shifted by $\pi/2$ in time. The Hilbert transform is applied along the temporal direction, and the resulting decomposition yields complex temporal modes that retain the analytic signal property. These modes can be interpreted as complex exponentials with instantaneous amplitude and phase, effectively representing the temporal evolution of wavepackets. Unlike other complex-valued decompositions, such as spectral POD, the modes in HPOD have instantaneous spectral content rather than being spectrally pure, enabling the analysis of modulation and intermittency phenomena in the data. In this study, HPOD is employed to investigate the temporal dynamics of the A1 and A2 screech modes. A brief overview of the method is provided here, while additional details on the mathematical formulation and implementation are provided in [27].

For statistically stationary flows, let $\boldsymbol{f} = (\boldsymbol{x},t)$ denote a random field composed of statistically independent snapshots. Proper orthogonal decomposition (POD) expresses $\boldsymbol{f} = (\boldsymbol{x},t)$ as a sum of orthonormal spatial modes $\psi_k(\boldsymbol{x})$ with corresponding temporal coefficients $a_k(t)$. The modes are ordered according to their associated energies η_k, in descending order, such that

$$\boldsymbol{f}(\boldsymbol{x},t) = \sum_{\mathrm{k}=1}^{\mathrm{K}} a_k(t)\,\psi_k(\boldsymbol{x}), \tag{2}$$

and is mathematically analogous to singular value decomposition and principal component analysis. Hilbert proper orthogonal decomposition incorporates phase information into the modes by replacing

$\boldsymbol{f} = (\boldsymbol{x}, t)$ with its associated analytic signal [28]

$$\boldsymbol{f}^a(\boldsymbol{x}, t) = \boldsymbol{f}(\boldsymbol{x}, t) + i\mathscr{H}[\boldsymbol{f}(\boldsymbol{x}, t)], \tag{3}$$

where $\mathscr{H}$ denotes the Hilbert transform of $\boldsymbol{f}(\boldsymbol{x}, t)$ with respect to time.
For time-resolved data, the Hilbert transform is applied with respect to time to compute the analytic signal $\boldsymbol{f}^a(\boldsymbol{x}, t)$. In order to perform HPOD, the two-point correlation of $\boldsymbol{f}^a(\boldsymbol{x}, t)$ in space is calculated:

$$C^a(\boldsymbol{x}, \boldsymbol{x}') = \int_T \boldsymbol{f}^a(\boldsymbol{x}, t)\, \boldsymbol{f}^a(\boldsymbol{x}', t)\, \mathrm{d}t, \tag{4}$$

where T denotes the temporal domain. The spatial modes and the corresponding energy are given by the eigendecomposition of $C^a(\boldsymbol{x}, \boldsymbol{x}')$

$$\int_S C^a(\boldsymbol{x}, \boldsymbol{x}')\, \psi^a(\boldsymbol{x}')\, \mathrm{d}\boldsymbol{x}' = \eta^a\, \psi^a(\boldsymbol{x}), \tag{5}$$

where S denotes the spatial domain. The temporal coefficients are computed by projecting $\boldsymbol{f}^a(\boldsymbol{x}, t)$ onto $\psi^a(\boldsymbol{x})$

$$a^a(t) = \int_S \boldsymbol{f}^a(\boldsymbol{x}, t)\, \psi^a(\boldsymbol{x})\, \mathrm{d}\boldsymbol{x}, \tag{6}$$

The spatial modes $\psi^a(\boldsymbol{x})$ are complex, with the imaginary component of $\psi^a(\boldsymbol{x})$ corresponding to a $\pm\pi/2$ phase shift of the real component. The instantaneous amplitude of the kth mode are defined by the real Re and imaginary Im components of $a^a(t)$ as

$$|a_k^a(t)| = \sqrt{\mathrm{Re}\{a_k^a(t)\}^2 + \mathrm{Im}\{a_k^a(t)\}^2}. \tag{7}$$

The instantaneous amplitude quantifies the strength of the mode at each instant. In the present study, the instantaneous amplitude is further smoothed using a moving-average filter and is denoted by $A_k(t)$.

4. Staging dynamics

This section examines the screech dynamics associated with A1–A2 mode staging. The frequency characteristics are first investigated using SPOD. Figure 2 shows the spectrum of the leading SPOD mode for the axisymmetric jet at $\mathrm{NPR} = 2.20$. The nondimensional frequency is expressed using the Strouhal number, $St = \frac{fD}{U_j}$, where D represents the jet exit diameter and U_j denotes the ideally expanded jet exit velocity. Two distinct, non-harmonically related peaks are observed at $St_1 = 0.606$ and $St_2 = 0.694$, corresponding to the axisymmetric A1 and A2 screech modes, respectively [7, 8]. The associated SPOD modes, presented in figure 3, are symmetric about the jet centreline and exhibit finite centreline amplitude, confirming the axisymmetric nature of both modes.

The presence of multiple peaks in the SPOD spectrum does not, by itself, indicate whether the corresponding screech modes coexist or alternate in time. To distinguish between these behaviours, the temporal evolution of the A1 and A2 modes is examined using the instantaneous modal amplitudes obtained from HPOD. Because both modes possess similar axisymmetric structures, they cannot be separated directly by HPOD. Therefore, the schlieren data are first reconstructed over narrow frequency bands using SPOD, isolating each screech mode prior to decomposition. HPOD is subsequently applied to each reconstructed dataset, allowing the leading HPOD mode to represent the temporal evolution of the corresponding screech mode. Figure 4 presents the instantaneous amplitudes of the A1 and A2 screech modes at $\mathrm{NPR} = 2.20$, where time is normalised by the period of the A2 mode, T. The modal amplitudes vary from nearly zero to approximately 5×10^4. The dominant behaviour consists of alternating periods of A1 and A2 dominance; however, the transitions occur over finite time intervals rather than instantaneously. During these intervals, both modes coexist at relatively low amplitudes (e.g. $t/T \approx 1800$, 9000, 14000 and 17400), indicating intermediate states in which neither mode is fully established. This behaviour differs from previous wavelet-based analyses

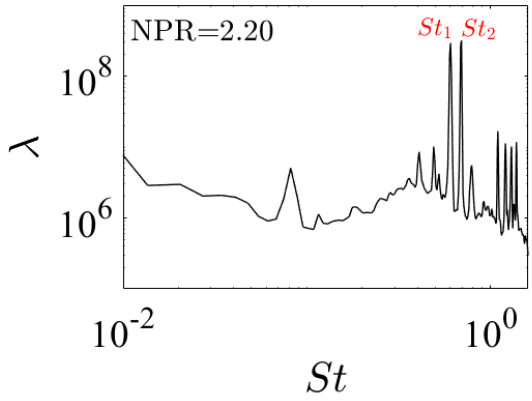


Figure 2 – SPOD eigenvalue spectra of the leading mode for the axisymmetric jet operating at $\mathrm{NPR} = 2.20$ corresponding to the A1–A2 mode transitions. $St_{1,2}$ denote the associated screech frequencies.

[14], which suggested abrupt on–off switching. Instead, the present results show that the staging process develops gradually over approximately $\mathcal{O}(100)$ screech cycles, with one mode decaying as the other grows. Two transition behaviours are observed. In the first, the dominant mode is completely replaced by the other (e.g. $t/T \approx 17000$). In the second, the modal amplitudes approach comparable levels before the transition reverses, allowing the initially dominant mode to recover (e.g. $t/T \approx 1800$).

The degree of mutual exclusivity between the two screech modes is further assessed using the joint probability density function (JPDF) of the normalised modal amplitudes, A^*_{A1} and A^*_{A2}, where each amplitude is normalised by its corresponding maximum value. As shown in figure 5, the highest probability density is concentrated along the coordinate axes, demonstrating that one mode typically exhibits a large amplitude while the other remains weak. The low-density region between the axes represents the relatively short periods during which both modes coexist at low amplitude. The relationship between the modal amplitudes is quantified using the Pearson correlation coefficient, ρ, calculated from A^*_{A1} and A^*_{A2}. The coefficient ranges from -1 (perfect anti-correlation) to 1 (perfect correlation), with $\rho = 0$ indicating no correlation. The measured value, $\rho(A^*_{A1}, A^*_{A2}) = -0.92$, demonstrates a strong anti-correlation between the A1 and A2 screech modes.

5. Mean-flow modification and mode staging

In §4., the staging process was characterised through the temporal evolution of the screech-mode amplitudes. We now investigate the physical mechanism responsible for this behaviour. Building on our previous study, which established that mean-flow modification is closely linked to the persistence of individual screech modes [17], the present analysis explores how changes in the mean flow influence the staging process. This requires a flow condition in which the screech modes alternate in a mutually exclusive manner, allowing the mean-flow state associated with each mode to be identified independently. In other words, a meaningful decomposition of the long-time mean flow is only possible when the screech resonance can effectively transition between active and inactive states. The mutually exclusive switching observed between the A1 and A2 modes provides precisely such a condition.

Figure 6 presents the leading HPOD spatial mode associated with the zero-frequency component, which represents the mean-flow modification. To isolate this component, the schlieren dataset is first reconstructed using only the zero-frequency SPOD mode before applying HPOD to the reconstructed field. Consequently, the leading HPOD mode captures the mean-flow distortion associated with $St = 0$. As shown in figure 6, the resulting spatial mode exhibits a shock-cell-like structure with finite amplitude along the jet centreline in both the real and magnitude fields.

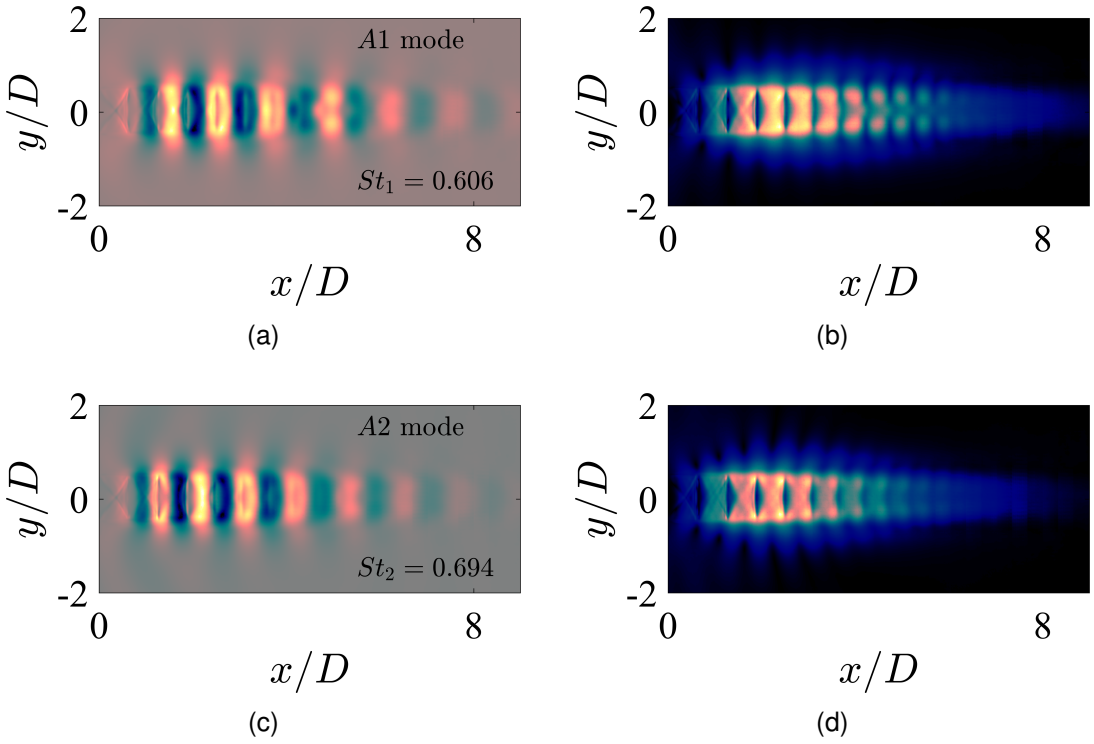


Figure 3 – Screech modes (St_1 and St_2) for the axisymmetric jet at $\mathrm{NPR} = 2.20$: (a, c) Real part of SPOD spatial mode. (b, d) Absolute value of SPOD spatial mode.

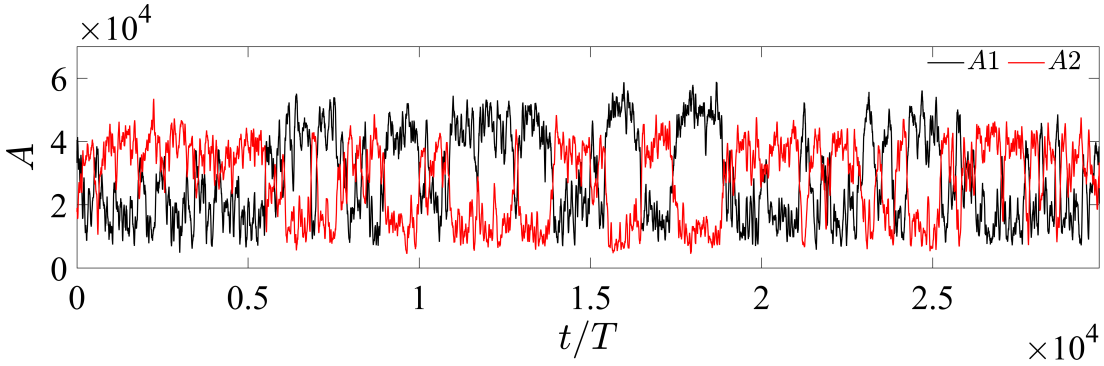


Figure 4 – Instantaneous amplitudes of the HPOD modes for the axisymmetric jet associated with modes A1 and A2 at $\mathrm{NPR} = 2.20$.

We next investigate the temporal relationship between the screech modes and the mode associated with mean-flow modification. Figure 7 shows the conditional amplitude of the zero-frequency mode, $A^*_{St=0}$, as a function of the normalised amplitudes of the A1 and A2 screech modes. The quantity $A^*_{St=0}$ varies between -1 and 1, where $A^*_{St=0} = 0$ represents a virtually unmodified base flow, while $A^*_{St=0} = \pm 1$ corresponds to the largest departure from this state. It is evident that when the screech modes have comparable amplitudes ($A^*_{A1} \approx A^*_{A2} \approx 0.5$), the zero-frequency amplitude remains close to zero, indicating minimal mean-flow modification. In contrast, as either the A1 or A2 mode becomes dominant ($A^*_{A1,A2} \approx 1$), the magnitude of the zero-frequency mode reaches its maximum value ($A^*_{St=0} = \pm 1$), demonstrating that the strongest mean-flow modification occurs when a single screech mode dominates.

Mean-flow modification is manifested through changes in the shock-cell spacing relative to the long-time mean flow. It is useful to distinguish between the long-time mean and the unmodified base flow. The long-time mean, $\bar{I}$, is computed from the complete dataset and therefore contains contributions from periods in which either the A1 or A2 screech mode is active. The unmodified base flow, by

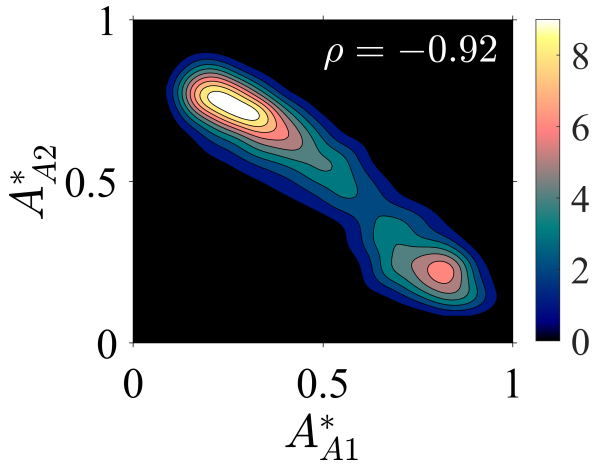


Figure 5 – Joint probability density functions of the instantaneous normalised amplitudes of the HPOD modes for the axisymmetric jet at $\mathrm{NPR} = 2.20$. The corresponding correlation coefficients are $\rho(A^*_{A1}, A^*_{A2}) = -0.92$.

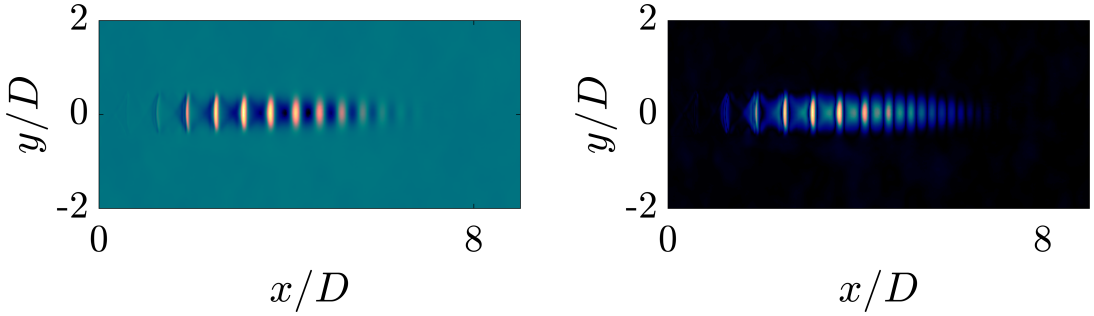


Figure 6 – Leading HPOD spatial mode, $\psi^a_{St=0}$, for the axisymmetric jet at $\mathrm{NPR} = 2.20$, corresponding to the mean-flow modification. (a) Real part of the mode ($\mathrm{Re}(\psi^a_{St=0})$). (b) Absolute value of the mode ($|\psi^a_{St=0}|$). The HPOD is applied to SPOD-based reconstructed data isolating the zero-frequency bin.

contrast, represents the flow in the absence of screech. Since the present dataset always contains at least one active screech mode, this reference state cannot be measured directly. To account for this limitation, we define an *actual mean flow* by correcting the long-time mean using the zero-frequency HPOD mode. The actual mean flow is expressed as

$$I_{\mathrm{Actual}}(t) = \bar{I} + A_{St=0}(t)\,\mathrm{Re}(\psi^a_{St=0})\,, \tag{8}$$

where $\bar{I}$ denotes the long-time mean flow, $\mathrm{Re}(\psi^a_{St=0})$ is the real component of the zero-frequency HPOD spatial mode (figure 6), and $A_{St=0}(t)$ is the corresponding (non-normalised) modal amplitude. The second term in equation 8 represents the instantaneous mean-flow correction associated with the shock-cell modification.

Two limiting states of $I_{\mathrm{Actual}}(t)$ are considered. The first corresponds to an A1-dominated state, characterised by $A^*_{A1} \approx 1$ and a positive maximum of $A^*_{St=0}$. The second corresponds to an A2-dominated state, where $A^*_{A2} \approx 1$ and $A^*_{St=0}$ reaches its negative maximum. These limiting conditions define the two short-time mean-flow states associated with the A1 and A2 screech modes. Figure 8 compares the long-time mean flow, obtained by averaging the entire schlieren dataset, with the two short-time mean-flow states. When the A1 mode dominates, the zero-frequency amplitude is positive ($A^*_{St=0} > 0$), corresponding to an extension in shock-cell spacing relative to the long-time mean (figure 8a). In contrast, dominance of the A2 mode is associated with a negative zero-frequency amplitude ($A^*_{St=0} < 0$), producing a contraction in shock-cell spacing (figure 8b). The departure from the long-time mean is more pronounced in the A1-dominated state, consistent with the asymmetric dis-

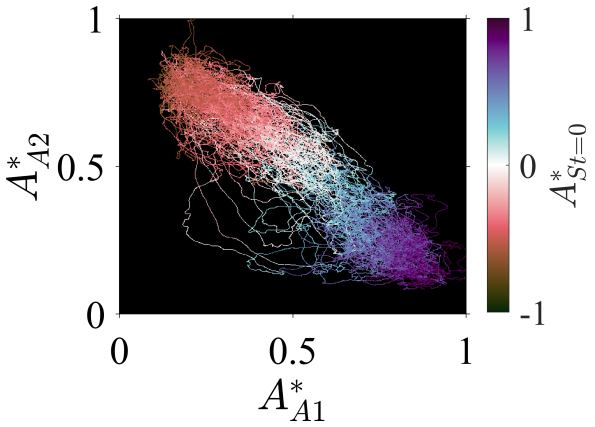


Figure 7 – Weighted joint histogram of the normalised amplitudes of modes A1 and A2 for the axisymmetric jet at $\mathrm{NPR} = 2.20$. The horizontal and vertical axes correspond to A^*_{A1} and A^*_{A2}, respectively, while the colour scale represents the normalised conditional amplitude of the zero-frequency component, $A^*_{St=0}$, conditioned on (A^*_{A1}, A^*_{A2}).

tribution of $A^*_{St=0}$ shown in figure 7, where the positive peak exceeds the magnitude of the negative peak, i.e. $|\max(A^*_{St=0})| > |\min(A^*_{St=0})|$. The evolution of the mean flow throughout a complete staging cycle can therefore be interpreted as a continuous variation in shock-cell spacing. When the A1 mode is fully established ($A^*_{A1} \approx 1$), the shock cells attain their greatest extension relative to the long-time mean (figure 8a). As the A1 amplitude decreases, the magnitude of the zero-frequency mode also diminishes, causing the actual mean flow to gradually approach the long-time mean. When the modal amplitudes become comparable ($A^*_{A1} \approx A^*_{A2} \approx 0.5$), the zero-frequency amplitude approaches zero ($A^*_{St=0} \approx 0$), such that the actual mean flow becomes nearly identical to the long-time mean ($I_{\mathrm{Actual}} \approx \bar{I}$). As the transition progresses further, the A2 mode continues to grow while the magnitude of the zero-frequency mode increases in the opposite direction, leading to a progressive contraction of the shock-cell spacing. The largest contraction occurs once the A2 mode becomes dominant ($A^*_{A2} \approx 1$), as illustrated in figure 8(b).

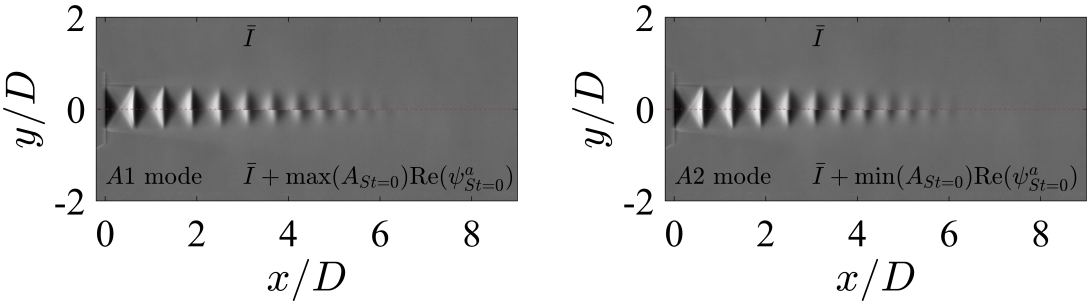


Figure 8 – Comparison between the long-time mean and short-time mean for the axisymmetric jet at $\mathrm{NPR} = 2.20$, with the two regions separated by the red dashed line. The upper section above the dashed line represents the long-time mean flow ($\bar{I}$), while the lower section shows the short-time mean flow modified by (a) $St_1 = 0.606$ and (b) $St_2 = 0.694$. $\max(A_{St=0})$ and $\min(A_{St=0})$ denote the maximum and minimum values of $A_{St=0}$ corresponding to $A_{St=0} > 0$ and $A_{St=0} < 0$, respectively.

Changes in the shock-cell spacing directly modify the shock-cell wavenumbers, k_{s_n}, which play a fundamental role in the screech resonance condition described by equation 1. These wavenumbers are commonly determined from temporally averaged PIV [7], schlieren [11], or numerical datasets [29] by performing an axial Fourier transform along the jet centreline to obtain the shock-cell wavenumber spectrum, as illustrated in figure 9. In the conventional approach, the characteristic wavenumbers, $k_{s_{n_{\bar{I}}}}$, are extracted from the long-time mean flow, $\bar{I}$. Since this mean is computed after the screech

has reached its limit-cycle state, it inherently includes the effects of mean-flow modification induced by the resonance.

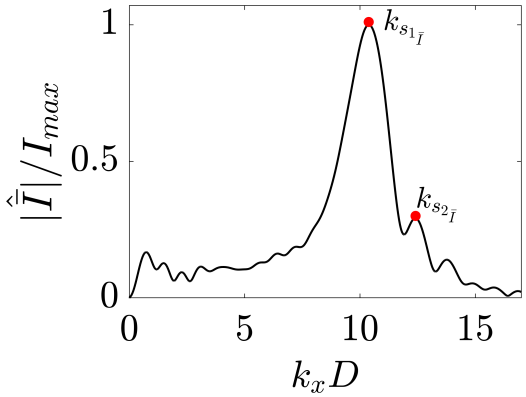


Figure 9 – Results of axial Fourier transforms performed at the centreline of the time-averaged shock structures image ($\bar{I}$) at $\mathrm{NPR} = 2.20$. Red dots represent k_{s_1} and k_{s_2}.

In the present study, the shock-cell wavenumbers are instead determined from the actual mean flow, I_{Actual}, thereby accounting for the influence of mean-flow modification. The deviation from the wavenumbers obtained using the conventional long-time mean is defined as

$$\Delta k_{s_n}(t) = k_{s_{n_{I_{\mathrm{Actual}}}}}(t) - k_{s_{n_{\bar{I}}}}. \tag{9}$$

The dependence of the shock-cell wavenumber variation on the screech-mode amplitudes is illustrated in figure 10. Here, negative values of Δk_{s_n} indicate an extension of shock-cell spacing relative to the long-time mean, whereas positive values correspond to a contraction relative to the long-time mean. Figure 10(a) shows that the primary shock-cell wavenumber, Δk_{s_1}, experiences its largest variation when the A2 mode is fully established ($A^*_{A2} \approx 1$), as highlighted by the purple region in the upper-left corner of the weighted joint histogram . When the A1 mode dominates, the change in Δk_{s_1} is substantially smaller, with a magnitude of roughly half that observed for the A2-dominated state. In contrast, figure 10(b) demonstrates that the largest variation in the secondary shock-cell wavenumber, Δk_{s_2}, occurs when the A1 mode is dominant ($A^*_{A1} \approx 1$), corresponding to the dark red region in the lower-right corner of the distribution. Conversely, the secondary wavenumber remains essentially unchanged ($\Delta k_{s_2} \approx 0$) when the A2 mode is dominant.

As discussed in §1., [30] demonstrated that the A1 screech mode satisfies the resonance condition through the interaction of the Kelvin–Helmholtz (KH) wavepacket with the primary shock-cell wavenumber, k_{s_1}, whereas the A2 mode is associated with the secondary shock-cell wavenumber, k_{s_2}. The results presented in figure 10 show that these two wavenumbers respond differently to mean-flow modification. Specifically, the largest changes in k_{s_1} occur when the A2 mode dominates, while the greatest variations in k_{s_2} are observed during A1-dominated states. This mode-dependent behaviour provides a physical explanation for the staging process. When the A1 mode is established, its nonlinear self-interaction modifies the mean flow such that the secondary shock-cell wavenumber, k_{s_2}, is shifted, whereas the primary wavenumber, k_{s_1}, remains comparatively unaffected. As a result, the resonance condition for the A2 mode is progressively satisfied, leading to its growth. Once the A2 mode becomes dominant, the process reverses. The mean-flow modification produced by the A2 mode preferentially alters k_{s_1} while leaving k_{s_2} largely unchanged, thereby re-establishing the resonance condition for the A1 mode. The system therefore alternates continuously between the two resonance states, completing the A1–A2 staging cycle.

To further assess the screech closure model described by equation 1, the shock-cell wavenumbers are evaluated using both the long-time and short-time mean flows. The comparison is presented in figure 11. Here, $k_{s_{n_{\bar{I}}}}$ denotes the shock-cell wavenumbers extracted from the long-time mean flow,

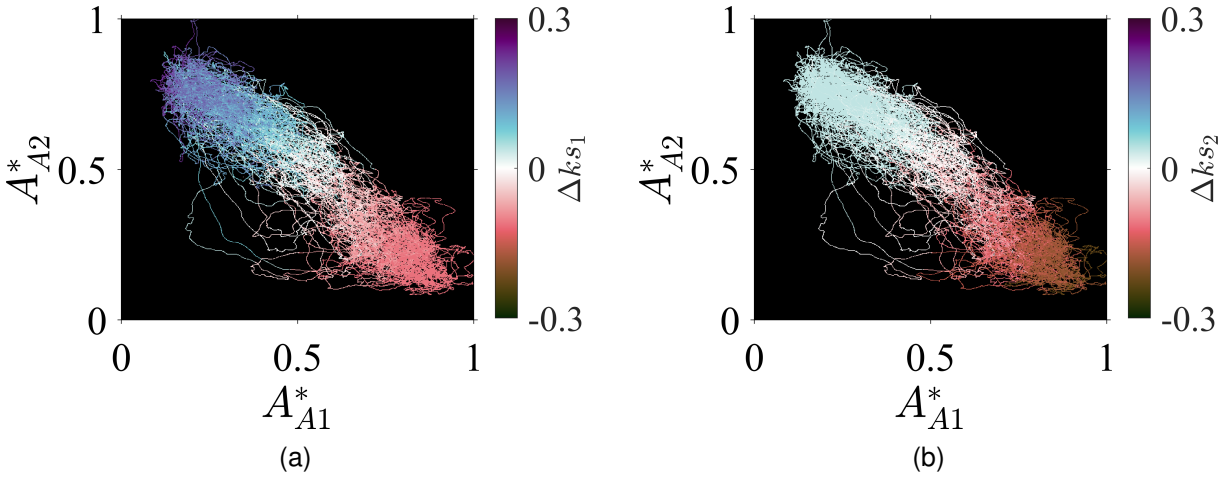


Figure 10 – Weighted joint histogram of the normalised amplitudes of modes A1 and A2 for the axisymmetric jet at NPR $= 2.20$. The horizontal and vertical axes correspond to A^*_{A1} and A^*_{A2}, respectively, while the contour levels represent the value of (a) $\Delta k_{s_1} = k_{s_1} - k_{s_{1_{\bar{I}}}}$. (b) $\Delta k_{s_2} = k_{s_2} - k_{s_{2_{\bar{I}}}}$.

whereas $k_{s_{n_{A1}}}$ and $k_{s_{n_{A2}}}$ are obtained from the short-time mean flows associated with the A1- and A2-dominated states, respectively. Following the relation $k_{sw} = k_{kh} - k_{GJM}$ proposed by [11], the standing-wave wavenumber, k_{sw}, is determined from the SPOD modes. This is achieved by first integrating the absolute value of the SPOD modes (figure 3b,d) in the radial direction to reduce sensitivity to radial variations, and then performing an axial Fourier transform to obtain the corresponding wavenumber spectra. The resulting standing-wave wavenumbers are denoted by $k_{sw_{A1}}$ for the A1 mode ($St_1 = 0.606$) and $k_{sw_{A2}}$ for the A2 mode ($St_2 = 0.694$).

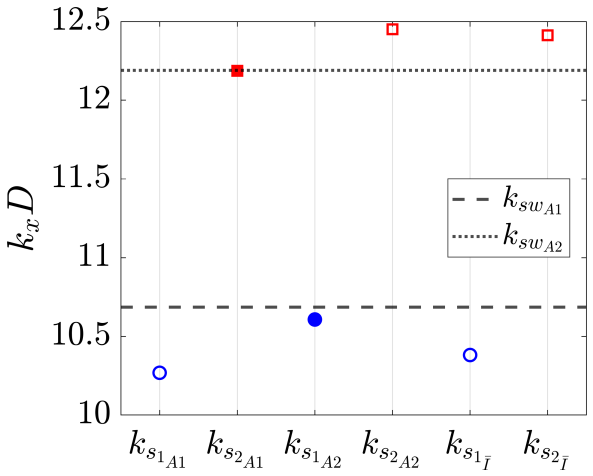


Figure 11 – Comparison of wavenumbers associated with k_{sw} and the primary (k_{s_1}) and secondary (k_{s_2}) peaks of the shock-cell structure for the axisymmetric jet at NPR $= 2.20$. Subscripts A1 and A2 denote short-time mean flows conditioned on the dominance of modes A1 and A2, respectively, while $\bar{I}$ denotes the long-time mean flow. Circles and squares indicate values of k_{s_1} and k_{s_2}, respectively.

Figure 11 demonstrates that the closest agreement between $k_{sw_{A1}}$ and the primary shock-cell wavenumber, k_{s_1}, is obtained when the short-time mean corresponding to the A2-dominated state (filled blue circles) is used. Likewise, the best agreement between $k_{sw_{A2}}$ and the secondary shock-cell wavenumber, k_{s_2}, is achieved using the short-time mean associated with the A1-dominated state (filled red squares). These results show that the screech closure model is more accurately described using the short-time mean flow than the conventional long-time mean. More importantly, the resonance condition for each mutually exclusive screech mode is most accurately recovered using the short-

time mean associated with the alternate mode. This provides strong quantitative evidence for the proposed staging mechanism, whereby each screech mode modifies the mean flow to establish the resonance condition required for the emergence of the other mode.

It should be noted that these results are preliminary, as they are derived using the long-time mean flow as the reference state rather than the true unmodified base flow, which is not accessible in the present experiments. A more definitive assessment of the shock-cell spacing variation requires direct measurements of the unmodified mean flow. In future work, we aim to obtain this reference state by suppressing the screech resonance using carefully positioned acoustic reflectors. The placement of these reflectors is critical, as they must eliminate the acoustic feedback responsible for screech while introducing minimal disturbance to the underlying flow. This approach will enable a direct comparison between the unmodified and screech-modified mean flows.

6. Conclusions

The present study investigated the physical mechanism underlying A1–A2 screech staging in an underexpanded axisymmetric supersonic jet using high-speed schlieren visualisations. SPOD and HPOD were employed to characterise both the spectral behaviour and the temporal evolution of the screech modes throughout the staging process.

The results show that transitions between the A1 and A2 screech modes are not instantaneous but occur over finite time intervals during which both modes coexist at low amplitude. Analysis of the zero-frequency HPOD mode demonstrates that the staging process is accompanied by continuous mean-flow modification, manifested as variations in the shock-cell spacing relative to the long-time mean flow. These changes are shown to affect the primary and secondary shock-cell wavenumbers differently, with the largest variation in k_{s_1} occurring during A2-dominated states and the largest variation in k_{s_2} occurring during A1-dominated states. Comparison of the measured standing-wave wavenumbers with the resonance closure model demonstrates that the screech frequencies are more accurately predicted using short-time mean flows than the conventional long-time mean flow. Furthermore, each screech mode is found to satisfy the resonance condition associated with the short-time mean of the alternate mode. These findings provide strong evidence that A1–A2 staging is governed by a self-sustaining feedback mechanism in which nonlinear mean-flow modification produced by one screech mode establishes the resonance condition required for the emergence of the other. While the present analysis uses the long-time mean flow as the reference state, future work will focus on obtaining the unmodified base flow by suppressing the screech resonance using carefully positioned acoustic reflectors. The proposed mechanism provides a new physical framework for understanding screech mode staging and lays the foundation for more accurate prediction of mode transitions in underexpanded supersonic jets.

7. Contact Author Email Address

Soudeh Mazharmanesh, mailto: soudeh.mazharmanesh@monash.edu

8. Copyright Statement

The authors confirm that they, and/or their company or organization, hold copyright on all of the original material included in this paper. The authors also confirm that they have obtained permission, from the copyright holder of any third party material included in this paper, to publish it as part of their paper. The authors confirm that they give permission, or have obtained permission from the copyright holder of this paper, for the publication and distribution of this paper as part of the ICAS proceedings or as individual off-prints from the proceedings.

References

[1] C. K. W. Tam. Supersonic jet noise. *Annual Review of Fluid Mechanics*, 27(1):17–43, 1995.

[2] G. Raman. Cessation of screech in underexpanded jets. *Journal of Fluid Mechanics*, 336:69–90, 1997.

[3] Wiesław Konopka, Małgorzata Pawlaczyk-Łuszczyńska, and Mariola Śliwińska-Kowalska. The influence of jet engine noise on hearing of technical staff. *Medycyna Pracy*, 65(5):583–592, 2014.

[4] A Powell. On the mechanism of choked jet noise. *Proceedings of the Physical Society. Section B*, 66(12):1039–1056, dec 1953.

[5] Christopher KW Tam and HK Tanna. Shock associated noise of supersonic jets from convergent-divergent nozzles. *Journal of Sound and Vibration*, 81(3):337–358, 1982.

[6] Christopher KW Tam, John M Seiner, and JC Yu. Proposed relationship between broadband shock associated noise and screech tones. *Journal of sound and vibration*, 110(2):309–321, 1986.

[7] Daniel Edgington-Mitchell, Tianye Wang, Petronio Nogueira, Oliver Schmidt, Vincent Jaunet, Daniel Duke, Peter Jordan, and Aaron Towne. Waves in screeching jets. *Journal of Fluid Mechanics*, 913:A7, 2021.

[8] Petrônio AS Nogueira, Vincent Jaunet, Matteo Mancinelli, Peter Jordan, and Daniel Edgington-Mitchell. Closure mechanism of the a1 and a2 modes in jet screech. *Journal of Fluid Mechanics*, 936, 2022.

[9] G. Raman. Advances in understanding supersonic jet screech: Review and perspective. *Progress in Aerospace Sciences*, 34(1):45 – 106, 1998.

[10] A. Powell, Y. Umeda, and R. Ishii. Observations of the oscillation modes of choked circular jets. *The Journal of the Acoustical Society of America*, 92(5):2823–2836, 1992.

[11] Daniel Edgington-Mitchell, Xiangru Li, Nianhua Liu, Feng He, Tsz Yeung Wong, Jacob Mackenzie, and Petronio Nogueira. A unifying theory of jet screech. *Journal of Fluid Mechanics*, 945:A8, 2022.

[12] SH Walker, SV Gordeyev, and FO Thomas. A wavelet transform analysis applied to unsteady aspects of supersonic jet screech resonance. *Experiments in fluids*, 22(3):229–238, 1997.

[13] Hao Shen and Christopher KW Tam. Three-dimensional numerical simulation of the jet screech phenomenon. *AIAA journal*, 40(1):33–41, 2002.

[14] M. Mancinelli, V. Jaunet, P. Jordan, and A. Towne. Screech-tone prediction using upstream-travelling jet modes. *Experiments in Fluids*, 60(1):22, 2019.

[15] Xiangru Li, Nianhua Liu, Pengfei Hao, Xiwen Zhang, and Feng He. Screech feedback loop and mode staging process of axisymmetric underexpanded jets. *Experimental Thermal and Fluid Science*, 122:110323, 2021.

[16] Tsz YM Wong, Michael N Stavropoulos, Jayson R Beekman, Aaron Towne, Petrônio AS Nogueira, Joel Weightman, and Daniel Edgington-Mitchell. Steady and unsteady coupling in twin weakly underexpanded round jets. *Journal of Fluid Mechanics*, 964:A2, 2023.

[17] Soudeh Mazharmanesh, Petrônio AS Nogueira, Joel Weightman, Brandon Yeung, Oliver T Schmidt, and Daniel Edgington-Mitchell. Triadic interaction and mean-flow deformation in screeching jets. *Journal of Fluid Mechanics*, 1039:A24, 2026.

[18] Christian E Willert, Daniel M Mitchell, and Julio Soria. An assessment of high-power light-emitting diodes for high frame rate schlieren imaging. *Experiments in fluids*, 53:413–421, 2012.

[19] John Leask Lumley. The structure of inhomogeneous turbulent flows. *Atmospheric turbulence and radio wave propagation*, pages 166–178, 1967.

[20] John L Lumey. *Stochastic tools in turbulence*. Elsevier, 2012.

[21] Aaron Towne, Oliver T Schmidt, and Tim Colonius. Spectral proper orthogonal decomposition and its relationship to dynamic mode decomposition and resolvent analysis. *Journal of Fluid Mechanics*, 847:821–867, 2018.

[22] O. T. Schmidt, A. Towne, G. Rigas, T. Colonius, and G. A. Brès. Spectral analysis of jet turbulence. *Journal of Fluid Mechanics*, 855:953–982, 2018.

[23] KR Sreenivasan. On the fine-scale intermittency of turbulence. *Journal of Fluid Mechanics*, 151:81–103, 1985.

[24] Romain Mathis, Nicholas Hutchins, and Ivan Marusic. Large-scale amplitude modulation of the small-scale structures in turbulent boundary layers. *Journal of Fluid Mechanics*, 628:311–337, 2009.

[25] Jochen Kriegseis, Matthias Kinzel, and Holger Nobach. Hilbert transform revisited–proper orthogonal decomposition applied to analytical signals of flow fields. In *14th International Symposium on Particle Image Velocimetry*, volume 1, 2021.

[26] Stefan L Hahn. Hilbert transforms in signal processing. *(No Title)*, 1996.

[27] Marco Raiola and Jochen Kriegseis. Hilbert proper orthogonal decomposition: a tool for educing advective wavepackets from flow field data. *arXiv preprint arXiv:2507.02487*, 2025.

[28] John D Horel. Complex principal component analysis: Theory and examples. *Journal of Applied Meteorology and Climatology*, 23(12):1660–1673, 1984.

[29] Yitao Wang, Xiangru Li, Juan Sheng, Feng He, Pengfei Hao, and Xiwen Zhang. Screech modes in underexpanded hot free jets. *Aerospace Science and Technology*, 157:109855, 2025.

[30] Petrônio AS Nogueira, José RLN Sirotto, Renato F Miotto, André VG Cavalieri, Julio A Cordioli, and William R Wolf. Acoustic radiation of subsonic jets in the vicinity of an inclined flat plate. *The Journal of the Acoustical Society of America*, 146(1):50–59, 2019.